universe

MDPI

*Article*

# Dark NLO Correction to Dark Photon Production at Lepton Colliders

**Jianming Zheng [1], Yi Li [1], Yusi Pan [2,*] and Mengchao Zhang [1,*]**

[1] Department of Physics and Siyuan Laboratory, Jinan University, Guangzhou 510632, China
[2] School of Electronic and Electrical Engineering, Shangqiu Normal University, Shangqiu 476000, China
* Correspondence: panyusi0406@foxmail.com (Y.P.); mczhang@jnu.edu.cn (M.Z.)

**Abstract**

In this work, we calculate the inclusive cross-section for the single dark photon production process in an electron–positron collider up to next-to-leading order (NLO). The dark photon studied in this work is embedded in a more complete dark Abelian Higgs model charged under a spontaneously broken $U(1)'$ gauge symmetry. The breaking of $U(1)'$ generates the mass of the dark photon. The inclusive cross-section contains $\sigma(e^+e^- \to \gamma A')$ and $\sigma(e^+e^- \to \gamma A's)$, with $A'/s$ being the dark photon/the dark Higgs, respectively. To remove the infrared (IR) divergence that appears at the high energy limit, virtual correction from the dark sector, which is the self-energy of dark photon, is also included. The cancellation of the IR divergences between the real correction and virtual correction makes the final NLO cross-section IR-safe. The phenomenological effect of this NLO correction is also briefly discussed.

**Keywords:** dark photon; dark Abelian Higgs model; lepton colliders; next-to-leading-order correction

## 1. Introduction

Dark photons (DPs), massive spin-1 vectors which couple to the visible particle via small kinetic mixing with a normal photon, are a popular assumption in New Physics beyond the Standard Model (SM) [1–11]. Phenomenologically, DPs are often viewed as a weak portal to the dark matter (DM) sector, and thus escape the increasingly stringent constraints on the DM parameter space [12–18].

DP (labeled as $A'$) can be detected through the kinetic mixing term by multiple experimental methods [19–32]. Current limits on DP detection can be found in [33–47]. Hadron colliders provide complementary constraints on dark photons. At the LHC, direct searches have been performed through prompt and displaced dilepton resonance channels, such as the inclusive LHCb searches for $A' \to \mu^+\mu^-$ and the CMS search for narrow dimuon resonances below the electroweak scale [44,48,49]. Additional hadron collider constraints arise from dark-sector topologies connected with Higgs and $Z$ boson decays [50–53]. In the very light and long-lived region, the forward LHC experiment FASER has also set strong limits on dark photons decaying to $e^+e^-$ [54]. These experimental studies are closely related to phenomenological analyses of lepton-jet signatures in hadron colliders [40,55,56]. It should be noted that most of the above work relies on a simple DP model setting, namely, that the properties of DP are determined by the DP mass $m_{A'}$ and kinetic mixing $\varepsilon$, but maintains an agnostic attitude towards the origin of the DP's mass. Therefore, the

Check for updates

Academic Editors: Douglas Singleton and Hermano Velten

Received: 28 March 2026
Revised: 14 May 2026
Accepted: 20 May 2026
Published: 22 May 2026

**Copyright:** © 2026 by the authors. Licensee MDPI, Basel, Switzerland. This article is an open access article distributed under the terms and conditions of the Creative Commons Attribution (CC BY) license.

phenomenological study of DP always ultimately boils down to an exclusion line on the $(m_{A'}, \varepsilon)$ plane.

Some phenomenological studies of DP have considered a more complete model [57–64], i.e., treating DP as a massive vector boson generated by the spontaneous symmetry breaking (SSB) of a dark-sector Abelian Higgs model. Then, in phenomenological studies, both DP and dark Higgs (labeled by $s$) are considered simultaneously[1].

Such a "DP + dark Higgs" framework leads to a richer phenomenology. For example, in the electron–positron collider, one can study the dark Higgsstrahlung process $e^+e^- \to A's$ instead of only considering the $e^+e^- \to \gamma A'$ process as in the "DP-only" model [57–62].

Recently, a previously overlooked process $e^+e^- \to \gamma A's$ was studied in an electron–positron collider [63,64]. This process is particularly important in the "fully invisible" case, where both $A'$ and $s$ decay into some invisible particles [63]. This is because if $A'$ and $s$ are both invisible, then the previously extensively studied $e^+e^- \to \gamma A'$ process would produce no signal at all, and thus $e^+e^- \to \gamma A's$ will actually become dominant.

As pointed out in [63], when the final state dark particles' masses are much smaller than the central energy $\sqrt{s}$ (i.e., $m_{A'}, m_s \ll \sqrt{s}$), $e^+e^- \to \gamma A's$ can be treated as real dark radiation correction to $e^+e^- \to \gamma A'$, with the final state sub-process $A' \to A's$ being the so-called dark final state radiation (FSR) [63]. The dark FSR process induces infrared (IR) divergence in the massless limit. To handle this problem, [63] uses the parton shower method to resum the dark FSR [66–69]. Furthermore, physical cross-section and distribution without IR divergence are obtained numerically using a modified version of PYTHIA8 [70].

In this article, however, we will use a fixed-order analytical calculation, which is different from [63], to directly eliminate IR divergence and obtain the physical cross-section. This analytical calculation can be viewed as a dark next-to-leading order (NLO) correction to $\sigma(e^+e^- \to \gamma A')$. To make the IR divergence disappear, the dark-sector virtual correction, which is actually the self-energy of DP, needs to be included. To our knowledge, this is the first time such a calculation has been performed in the literature. We will also briefly discuss how this dark NLO correction affects current BaBar limits on DP.

In the next section, we introduce the model that we want to study. Section 3 is dedicated to the calculation of the cross-section. In Section 4, we use invisible DP search at BaBar as an example to show the effect of dark NLO correction. We conclude this work in Section 5.

## 2. Dark Abelian Higgs Model

The model we will study is a dark Abelian Higgs model that links to the SM via kinetic mixing. After rotating to the mass-eigenstate, the Lagrangian is as follows $((+,-,-,-)$ metric):

$$\mathcal{L} = (D_\mu S)^\dagger D^\mu S - \frac{1}{4} F'_{\mu\nu} F'^{\mu\nu} + \mu^2 S^\dagger S - \frac{1}{4}\lambda (S^\dagger S)^2 - \varepsilon e J^{\mathrm{EM}}_\mu A'^\mu \tag{1}$$

with $S$ being the dark Higgs charged under $U(1)'$, $D_\mu \equiv \partial_\mu + i g' A'_\mu$ being the covariant derivative, $g'$ being the $U(1)'$ coupling constant, $F'_{\mu\nu} \equiv \partial_\mu A'_\nu - \partial_\nu A'_\mu$ being the field strength of DP, and $J^{\mathrm{EM}}_\mu$ being the electromagnetic current. $\varepsilon$ is the kinetic mixing parameter, which is generally much smaller than 1.

Negative mass term $-\mu^2$ breaks the $U(1)'$ symmetry and gives $S$ a vacuum expected value (VEV) $v$. Then, $S$ can be expanded as

$$S = \frac{1}{\sqrt{2}}(v + s + ia) \tag{2}$$

with $v \equiv 2\mu/\sqrt{\lambda}$, $s$ as the physical dark Higgs, and $a$ as the Goldstone. Under unitary gauge, the Goldstone and ghost are decoupled, and the squared masses of the dark Higgs and the DP are

$$m_s^2 = \frac{1}{2}\lambda v^2 \ , \ m_{A'}^2 = g'^2 v^2 \tag{3}$$

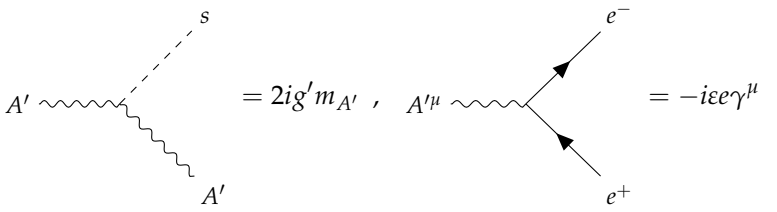
In this work, we will study the invisible DP. Furthermore, we also require dark Higgs to be invisible at collider. To achieve this fully invisible scenario, one generally needs to include some invisible light particles in the model. However, this part is not directly related to the main focus of this work, so we will not explicitly describe it but simply assume that DP and dark Higgs in our model are invisible in the collider[2].

For later convenience, as an analogy to the QED fine structure constant $\alpha \equiv e^2/4\pi$, we define a dark fine structure constant $\alpha' \equiv g'^2/4\pi$. We will choose $\{\varepsilon, m_s, m_{A'}, \alpha'\}$ as the input parameters for our model.

## 3. Cross-Section Calculation

In this section, we perform a detailed calculation for the cross-section of $e^+e^- \to \gamma A'$ and its dark NLO correction $e^+e^- \to \gamma A's$. Both the $A'$ and $s$ are invisible in the collider, and thus processes $e^+e^- \to \gamma A'$ and $e^+e^- \to \gamma A's$ actually produce the same collider signal, i.e., single photon + missing energy. If no further kinematic cuts are performed, then these two processes can be combined and one can obtain an inclusive cross-section $\sigma(e^+e^- \to \gamma A' + X)$. We will show that the IR divergence cancellation happens between the virtual correction of $e^+e^- \to \gamma A'$ and $e^+e^- \to \gamma A's$.

In addition to the SM interaction, there are two vertexes that will enter our calculation:




(4)

Amplitudes for processes $e^+e^- \to \gamma A'$ and $e^+e^- \to \gamma A's$ are labeled by $i\mathcal{M}_0$ and $i\mathcal{M}_R$, respectively. And the dark virtual correction to $i\mathcal{M}_0$, which comes from the self-energy of final state $A'$, is labeled by $i\mathcal{M}_V$. One will find the following dependence of amplitude on coupling strengths:

$$i\mathcal{M}_0 \propto \varepsilon\alpha \ , \ i\mathcal{M}_R \propto \varepsilon\alpha\alpha'^{1/2} \ , \ i\mathcal{M}_V \propto \varepsilon\alpha\alpha' \tag{5}$$

### 3.1. Amplitudes

In this subsection, we present the expressions for $i\mathcal{M}_0$, $i\mathcal{M}_R$, and $i\mathcal{M}_V$.

The amplitude for tree-level process $e^+e^- \to \gamma A'$, as shown in Figure 1, is

$$i\mathcal{M}_0 = -i\varepsilon e^2 \bar{v}(p_2)\left[\not{\epsilon}(k_2)\frac{1}{\not{p}_1 - \not{k}_1 - m_e}\not{\epsilon}(k_1) + \not{\epsilon}(k_1)\frac{1}{\not{k}_1 - \not{p}_2 - m_e}\not{\epsilon}(k_2)\right]u(p_1) \tag{6}$$

Momentums for the initial electron and positron are labeled by $p_{1,2}$, with $p_{1,2} = (\sqrt{s}/2, 0, 0, \pm\sqrt{s/4 - m_e^2})$ and $m_e$ the electron mass. Here, we miss the polarization index for concision. $k_1$ and $k_2$ are the momentum of the DP and photon, respectively.

The amplitude for tree-level process $e^+e^- \to \gamma A's$, as shown in Figure 2, is

$$i\mathcal{M}_R = -i\varepsilon e^2 \frac{2g' m_{A'}}{q^2 - m_{A'}^2} \bar{v}(p_2) \left[ \not{\epsilon}(k_2) \frac{1}{\not{p}_1 - \not{q} - m_e} \not{\epsilon}(k_{A'}) + \not{\epsilon}(k_{A'}) \frac{1}{\not{q} - \not{p}_2 - m_e} \not{\epsilon}(k_2) \right] u(p_1) \tag{7}$$

Here, $k_{A'}$ is the momentum of final state DP, and $q \equiv k_{A'} + k_s$ is the momentum of intermediate state DP. The $q^\mu q^\nu$ part in the DP propagator does not contribute to the amplitude, and thus we can remove it.

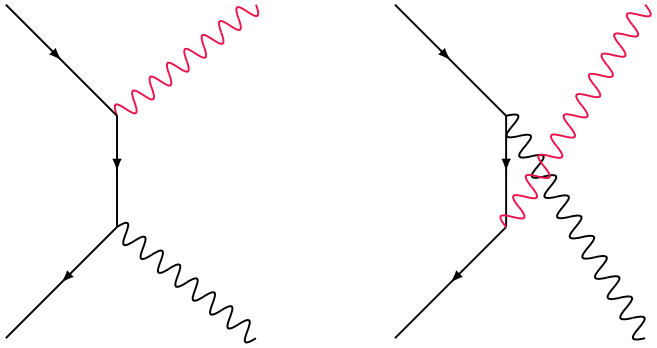


**Figure 1.** Black arrowed line is electron. Black wave line is photon. Red wave line is dark photon. These two diagrams correspond to amplitude $i\mathcal{M}_0$.

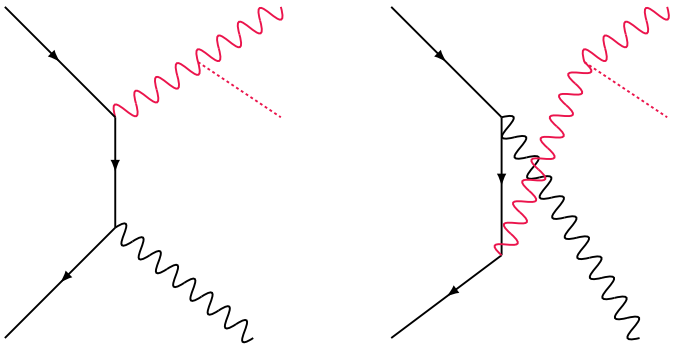


**Figure 2.** Black arrowed line is electron. Black wavy line is photon. Red wavy line is dark photon. Red dotted line is dark Higgs. These two diagrams correspond to amplitude $i\mathcal{M}_R$.

The amplitude for the loop level process $e^+e^- \to \gamma A'$, as shown in Figure 3, is

$$i\mathcal{M}_V = -i(\mathcal{Z}_{A'}^{1/2} - 1)\varepsilon e^2 \bar{v}(p_2) \left[ \not{\epsilon}(k_2) \frac{1}{\not{p}_1 - \not{k}_1 - m_e} \not{\epsilon}(k_1) + \not{\epsilon}(k_1) \frac{1}{\not{k}_1 - \not{p}_2 - m_e} \not{\epsilon}(k_2) \right] u(p_1) \tag{8}$$

with $\mathcal{Z}_{A'}$ as the wave function renormalization factor of DP.

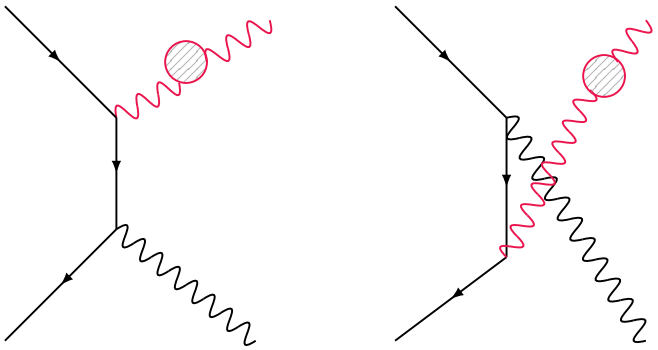


**Figure 3.** Black arrowed line is electron. Black wavy line is photon. Red wavy line is dark photon. Red bulb is the self-energy correction for dark photon. These two diagrams correspond to amplitude $i\mathcal{M}_V$.

https://doi.org/10.3390/universe12060153

$\mathcal{Z}_{A'}$ relates to the DP self-energy correction $\Pi_{A'}(p^2)$ via

$$\mathcal{Z}_{A'} = \left(1 - \frac{d}{dp^2}\Pi_{A'}(p^2)\Big|_{p^2=m_{A'}^2}\right)^{-1} \tag{9}$$

The prescription used here should not be confused with a complete on-shell renormalization scheme. We identify $m_{A'}$ with the physical pole mass at the order considered, while the one-loop self-energy quoted below is ultraviolet-subtracted in the $\overline{\text{MS}}$ of Ref. [71]. We do not impose the additional on-shell field-renormalization condition that sets the pole residue to unity. Instead, the finite pole-residue factor $\mathcal{Z}_{A'}$ is kept explicitly as the LSZ factor for the external dark photon. At the one-loop level, $\Pi_{A'}(p^2)$ is proportional to $\alpha'$; thus, in Equation (8), we can replace factor $(\mathcal{Z}_{A'}^{1/2} - 1)$ by $\frac{1}{2}\frac{d}{dp^2}\Pi_{A'}(p^2)\Big|_{p^2=m_{A'}^2}$. Here, we give the concrete expression of $\frac{d}{dp^2}\Pi_{A'}(p^2)\Big|_{p^2=m_{A'}^2}$, which is derived from [71]

$$\begin{aligned}\frac{d}{dp^2}\Pi_{A'}(p^2)\Big|_{p^2=m_{A'}^2} &= \frac{\alpha'}{2\pi}\frac{1}{36\sqrt{4r-1}}\Bigg[\sqrt{4r-1}\Bigg(6\ln(\frac{m_{A'}^2}{\mu^2}) + 62 - 36\frac{1}{r} + 12\frac{1}{r^2} \\ &\quad +(-36 + 54\frac{1}{r} - 27\frac{1}{r^2} + 6\frac{1}{r^3})\ln(r)\Bigg) \\ &\quad +6(36 - 32\frac{1}{r} + 13\frac{1}{r^2} - 2\frac{1}{r^3})(\tan^{-1}(\frac{1}{\sqrt{4r-1}}) + \tan^{-1}(\frac{1-2r}{\sqrt{4r-1}}))\Bigg]\end{aligned} \tag{10}$$

with $r \equiv m_{A'}^2/m_s^2$ being the ratio of two mass squares, and $\mu$ being the renormalization scale, which is around $\sqrt{s}$. In this work, we use Equation (10) on the real-valued branch $r > 1/4$, which is also the region where the dark Higgs is stable against the decay $s \to A'A'$ in the minimal dark Abelian Higgs sector. It is obvious that there is an IR divergent term that is proportional to $\ln(m_{A'}^2/\mu^2)$, i.e., this term will be divergent when $m_{A'}^2 \to 0$. In the next subsection, we will see how this virtual IR divergence cancels with the real IR divergence in process $e^+e^- \to \gamma A's$.

For later convenience, we define a virtual correction factor as

$$\mathcal{C}_V \equiv \frac{1}{2}\frac{d}{dp^2}\Pi_{A'}(p^2)\Big|_{p^2=m_{A'}^2} \tag{11}$$

and thus, we have $i\mathcal{M}_V = \mathcal{C}_V i\mathcal{M}_0$.

### *3.2. Inclusive Cross-Section*

As we explained before, the inclusive cross-section $\sigma(e^+e^- \to \gamma A' + X)$ should be IR-safe. In this subsection, we show how the virtual and real IR divergences cancel each other.

Up to the NLO order, inclusive $\sigma(e^+e^- \to \gamma A' + X)$ can be expressed as

$$\begin{aligned}\sigma(e^+e^- \to \gamma A' + X) &= \frac{1}{4\sqrt{(p_1\cdot p_2)^2 - m_e^4}}\left(\int d\Pi_2\left(\overline{|\mathcal{M}_0|^2} + \overline{\mathcal{M}_0\mathcal{M}_V^\dagger} + \overline{\mathcal{M}_0^\dagger\mathcal{M}_V}\right) + \int d\Pi_3\overline{|\mathcal{M}_R|^2}\right) \\ &= \frac{1}{4\sqrt{(p_1\cdot p_2)^2 - m_e^4}}\left((1 + \mathcal{C}_V + \mathcal{C}_V^*)\int d\Pi_2\overline{|\mathcal{M}_0|^2} + \int d\Pi_3\overline{|\mathcal{M}_R|^2}\right) \\ &= \sigma_V(e^+e^- \to \gamma A') + \sigma_R(e^+e^- \to \gamma A's)\end{aligned} \tag{12}$$

with $d\Pi_2$ and $d\Pi_3$ being the two-body and three-body phase-space measures. And $\overline{|\mathcal{M}|^2}$ is the spin-averaged amplitude square:

$$\overline{|\mathcal{M}|^2} = \frac{1}{4}\sum_{\text{spin}}|\mathcal{M}|^2 \tag{13}$$

The expressions for $\sigma_V(e^+e^- \to \gamma A')$ and $\sigma_R(e^+e^- \to \gamma A's)$ can be obtained through lengthy but direct calculations. $\sigma_V(e^+e^- \to \gamma A')$ can be written in a compact form as

$$\sigma_V(e^+e^- \to \gamma A') = (1 + \mathcal{C}_V + \mathcal{C}_V^*)\,\sigma_0, \tag{14}$$

where $\sigma_0$ is the tree-level cross-section for $e^+e^- \to \gamma A'$:

$$\begin{aligned} &\sigma_0(e^+e^- \to \gamma A') \\ &= 4\pi\epsilon^2\alpha^2\,\frac{2\sqrt{s}\left(m_{A'}^4 - 4m_{A'}^2 m_e^2 - 8m_e^4 + 4m_e^2 s + s^2\right)\tanh^{-1}\left(\sqrt{1-\frac{4m_e^2}{s}}\right) - \sqrt{s-4m_e^2}\left(m_{A'}^4 + s(4m_e^2+s)\right)}{\sqrt{s}\,(m_{A'}^2 - s)^2(s-4m_e^2)}. \end{aligned} \tag{15}$$

Three-body phase space for process $e^+e^- \to \gamma A's$ is more complicated. One can first integrate out the angle variables to convert the cross-section into an integral over the photon energy $E_\gamma$:

$$\begin{aligned} \sigma_R(e^+e^- \to \gamma A's) &= \int_{E_{\rm cut}}^{E_{\rm max}} dE_\gamma\,\hat{\sigma}_0\Big(s, q^2\Big)\,\frac{2\alpha'\sqrt{s}\,m_{A'}^2}{\pi\,q^2\,(q^2 - m_{A'}^2)^2}\,\lambda^{1/2}(q^2, m_{A'}^2, m_s^2)\left[1 + \frac{\lambda(q^2, m_{A'}^2, m_s^2)}{12\,m_{A'}^2\,q^2}\right], \\ &\text{where}\quad q^2 = s - 2E_\gamma\sqrt{s}\quad\&\quad E_{\rm max} = \frac{s - (m_{A'} + m_s)^2}{2\sqrt{s}}. \end{aligned} \tag{16}$$

$\lambda$ function in the above equation is given by

$$\lambda(x, y, z) = x^2 + y^2 + z^2 - 2xy - 2xz - 2yz \tag{17}$$

And we also define the "off-shell DP" cross-section for convenience:

$$\begin{aligned} &\hat{\sigma}_0(s, Q^2) \\ &= 4\pi\epsilon^2\alpha^2\,\frac{2\sqrt{s}\left[Q^4 - 4Q^2 m_e^2 - 8m_e^4 + 4m_e^2 s + s^2\right]\operatorname{arctanh}\sqrt{1-\frac{4m_e^2}{s}} - \sqrt{s-4m_e^2}\left[Q^4 + s(4m_e^2+s)\right]}{\sqrt{s}\,(Q^2 - s)^2(s-4m_e^2)}. \end{aligned} \tag{18}$$

And it should be noticed that $\sigma_0 = \hat{\sigma}_0(s, m_{A'}^2)$. Furthermore, for the 3-body process, we require a lower energy cut $E_{\rm cut}$ on the final state photon. This is because the "single photon + missing energy" signal at collider requires the final state photon to be energetic enough.

The integration of $E_\gamma$ in Equation (16) can be done and thus, one can obtain a closed form. However, this expression will be unnecessarily complicated. In Section 4, we will evaluate $\sigma_R(e^+e^- \to \gamma A's)$ numerically.

### 3.3. IR Safety

As we have shown in Equation (10), the virtual correction actually brings IR divergence. This IR divergence[3] should be cancelled by the real correction to obtain an IR-safe inclusive cross-section. This is the KLN-type cancellation of mass singularities for sufficiently inclusive observables [72,73]. In the present dark-sector correction, the singular part of the real emission originates from the region in which the final-state dark photon and dark Higgs form an unresolved collinear dark system. To clarify this point, in this subsection, we abstract the IR divergent part in $\sigma_V$ and $\sigma_R$.

The IR divergent part of $\sigma_V$ can be easily obtained from Equations (10) and (14):

$$\sigma_V^{\rm IR} = \frac{\alpha'}{12\pi}\ln\left(\frac{m_{A'}^2}{\mu^2}\right)\sigma_0 \tag{19}$$

To extract the IR divergent part of $\sigma_R$, we start from Equation (16) and change the integration variable from $E_\gamma$ to $q^2 = s - 2E_\gamma\sqrt{s}$. Since $dE_\gamma = -\frac{dq^2}{2\sqrt{s}}$, we obtain

$$\sigma_R = \int_{(m_{A'}+m_s)^2}^{q^2_{\rm cut}} dq^2 \hat{\sigma}_0(s,q^2)\, \frac{\alpha' m^2_{A'}}{\pi\, q^2\, (q^2 - m^2_{A'})^2}\, \lambda^{1/2}(q^2, m^2_{A'}, m^2_s) \left[1 + \frac{\lambda(q^2, m^2_{A'}, m^2_s)}{12\, m^2_{A'}\, q^2}\right], \quad (20)$$

where $q^2_{\rm cut} \equiv s - 2E_{\rm cut}\sqrt{s}$.

Now, we consider the limit $m_{A'} \to 0$ while keeping $r \equiv m^2_{A'}/m^2_s$ fixed. Defining the dimensionless variable $x \equiv q^2/m^2_{A'}$, we have

$$\sigma_R = \frac{\alpha'}{\pi} \int_{x_{\rm min}}^{x_{\rm max}} dx\, \hat{\sigma}_0(s, m^2_{A'}x)\, \frac{\sqrt{\Lambda_r(x)}}{x(x-1)^2} \left[1 + \frac{\Lambda_r(x)}{12x}\right], \quad (21)$$

with

$$x_{\rm min} = \left(1 + \frac{1}{\sqrt{r}}\right)^2, \qquad x_{\rm max} = \frac{q^2_{\rm cut}}{m^2_{A'}}, \quad (22)$$

and the dimensionless function

$$\Lambda_r(x) = x^2 + 1 + \frac{1}{r^2} - 2x - \frac{2x}{r} - \frac{2}{r}. \quad (23)$$

The value of $x_{\rm min}$ is about 1; thus, the logarithmic IR contribution originates from the large-$x$ region, i.e., from the vicinity of $x_{\rm max}$. $x_{\rm max}$ tends to infinity when $m_{A'} \to 0$. This means that in order to obtain IR divergence, we should expand the integrand of (21) by $1/x$. For a large $x$, one has

$$\sqrt{\Lambda_r(x)} = x - \left(1 + \frac{1}{r}\right) + \mathcal{O}\left(\frac{1}{x}\right), \qquad 1 + \frac{\Lambda_r(x)}{12x} = 1 + \frac{x}{12} - \frac{1}{6}\left(1 + \frac{1}{r}\right) + \mathcal{O}\left(\frac{1}{x}\right). \quad (24)$$

And hence,

$$\frac{\sqrt{\Lambda_r(x)}}{x(x-1)^2}\left[1 + \frac{\Lambda_r(x)}{12x}\right] = \frac{1}{12x} + \mathcal{O}\left(\frac{1}{x^2}\right). \quad (25)$$

On the other hand, in the $m_{A'} \to 0$ limit, the off-shell cross-section $\hat{\sigma}_0(s, m^2_{A'}x)$ can be expanded as

$$\hat{\sigma}_0(s, m^2_{A'}x) = \sigma_0 + \mathcal{O}(m^2_{A'}x) \quad (26)$$

It is easy to see that the integral over the second term is finite, because

$$\int^{x_{\rm max}} dx\, \mathcal{O}(m^2_{A'}x)\, \frac{1}{x} \sim \mathcal{O}(m^2_{A'}x_{\rm max}) \sim \mathcal{O}(q^2_{\rm cut}) \quad (27)$$

So we can approximate $\hat{\sigma}_0(s, m^2_{A'}x)$ by $\sigma_0$ when extracting the IR divergence:

$$\sigma_R^{\rm IR} = \frac{\alpha'}{12\pi}\sigma_0 \int^{x_{\rm max}} \frac{dx}{x} = -\frac{\alpha'}{12\pi} \ln\left(\frac{m^2_{A'}}{q^2_{\rm cut}}\right)\sigma_0. \quad (28)$$

Here, we explain why the IR divergence in $\sigma_R^{\rm IR}$ actually comes from the collinear region. The invariant mass of the invisible dark system is $q^2 = (p_{A'} + p_s)^2$. In the quasi-collinear splitting $A'^*(q) \to A'(p) + s(k)$, one may write

$$q^2 = \frac{k_\perp^2 + (1-z)m_{A'}^2 + z m_s^2}{z(1-z)}, \tag{29}$$

where $z$ is the longitudinal momentum fraction carried by the final dark photon and $k_\perp$ is the relative transverse momentum of the two dark particles. Therefore, in the hierarchy $m_{A'}^2, m_s^2 \ll q^2 \ll s$, the large-$x$ integral is equivalently the collinear integral:

$$\frac{dq^2}{q^2} \simeq \frac{dk_\perp^2}{k_\perp^2}. \tag{30}$$

The logarithm in Equation (28) is thus the usual mass-regulated collinear logarithm associated with unresolved dark-sector splitting.

This also explains why the cancellation of the mass singularity is not spoiled by ordinary mono-photon cuts, provided the observable remains inclusive with respect to the unresolved dark-sector radiation. The detector measures the visible photon and the total missing momentum, but it does not resolve the internal collinear structure of the invisible $A's$ system. Such cuts can change the upper scale $q_{\rm cut}^2$ and the finite accepted rate, but not the universal coefficient of the mass singularity that cancels the corresponding virtual contribution.

The sum of (19) and (28) gives

$$\sigma_V^{\rm IR} + \sigma_R^{\rm IR} = \frac{\alpha'}{12\pi} \ln\left(\frac{q_{\rm cut}^2}{\mu^2}\right)\sigma_0 \,, \tag{31}$$

which is finite in the $m_{A'} \to 0$ limit. Thus, we have analytically proven that the inclusive cross-section $\sigma(e^+e^- \to \gamma A' + X)$ is IR-safe.

## 4. Numerical Results and Implication for BaBar Limit

In this section, we first obtain the numerical solution of the inclusive section $\sigma(e^+e^- \to \gamma A' + X)$ by numerically integrating Equation (16). The central energy $\sqrt{s}$ is chosen to be the same as the BaBar setting [35], which is 10.58 GeV. For the final-state photon energy lower bound $E_{\rm cut}$, we also follow the BaBar report [35] and let $E_{\rm cut} = 3$ GeV. Renormalization scale $\mu$ is fixed to the central energy, i.e., $\mu = \sqrt{s}$. Furthermore, we choose mass ratio $r = 1$ for illustration in Figure 4.

In Figure 4, we show the ratio $\frac{\sigma(e^+e^- \to \gamma A' + X)}{\sigma_0(e^+e^- \to \gamma A')} - 1$ as a function of DP mass $m_{A'}$[4]. As one can see, the cross-section ratio increases as $m_{A'}$ decreases from 3 GeV, which is because the final-state phase space gradually becomes larger. Then, when $m_{A'}$ is sufficiently small, this ratio essentially remains unchanged, which is also a physical consequence. To clearly illustrate the cancellation between the virtual and real corrections, we also plotted the ratios of these two corrections to $\sigma_0$ in the figure. We can see that both the virtual and real corrections actually increase as $m_{A'}$ approaches zero. However, the mutual cancellation of their IR divergence parts provides a physically IR-safe result.

To address the dark-Higgs-mass dependence, we also scan representative values $r = 1/3, 1/2, 1, 2, 3$. All these choices satisfy $r > 1/4$, so that the self-energy expression in Equation (10) is evaluated on the same real branch. The result is shown in Figure 5.

In Figure 5, we present the the normalized ratio $(\sigma_{\rm NLO}/\sigma_0 - 1)/\alpha'$ (with $\sigma_{\rm NLO} = \sigma_V + \sigma_R$) as functions of $m'_A$ with different $r$ values. The fixed-order correction remains smooth and perturbative in the displayed range. The dependence on $r$ is not

monotonic: in the low-mass region, the largest correction among the displayed benchmarks occurs around the intermediate value $r = 1/2$, while it is smaller for both $r = 1/3$ and for larger values of $r$. This behavior reflects the competition between the real-emission phase space for a lighter dark Higgs and the finite virtual residue correction. For larger $r$, the finite virtual term becomes increasingly negative and partly overcompensates for the real-emission phase-space enhancement, so that the net correction decreases.

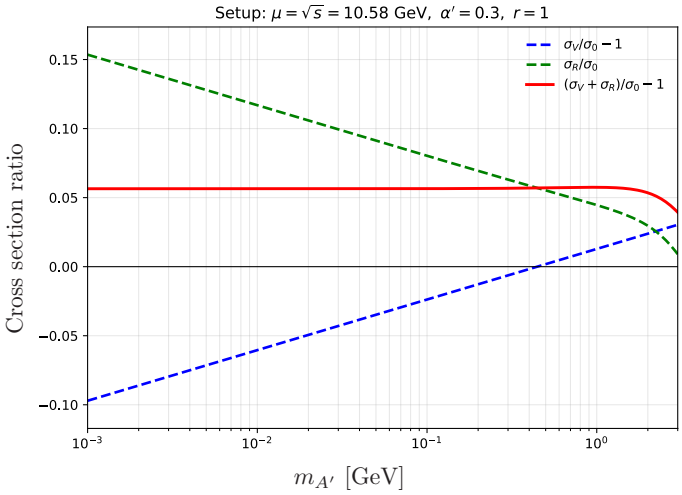



**Figure 4.** Relative NLO corrections as functions of $m_{A'}$. Green dashed line is the ratio between real correction and tree-level cross-section. Blue dashed line is the ratio between virtual correction and tree-level cross-section. Red line is the ratio between complete NLO correction and tree-level cross-section.

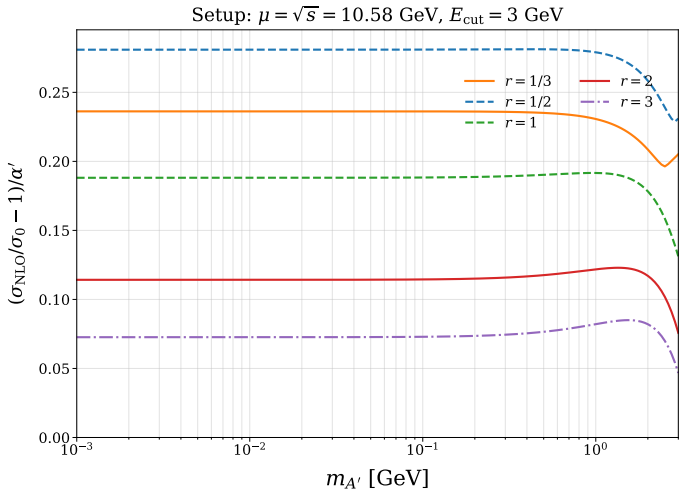



**Figure 5.** Normalized NLO correction $(\sigma_{\rm NLO}/\sigma_0 - 1)/\alpha'$ as a function of $m_{A'}$ for $r = m_{A'}^2/m_s^2 = 1/3, 1/2, 1, 2, 3$. The setup is $\sqrt{s} = 10.58$ GeV, $E_{\rm cut} = 3$ GeV, and $\mu = \sqrt{s}$.

Next, we briefly discuss how this correction to the DP production cross-section will affect DP detection on electron–positron colliders. We will still take the BaBar experiment as an example. BaBar's detection of invisible DP is mainly based on the kinetic variable squared missing mass $M_X^2$, which is defined as

$$M_X^2 = (p_{e^+} + p_{e^-} - k_\gamma)^2 = s - 2E_\gamma^* \sqrt{s} \tag{32}$$

Precisely speaking, the $M_X^2$ distribution of LO process $e^+e^- \to \gamma A'$ is different from the $M_X^2$ distribution of the NLO inclusive process $e^+e^- \to \gamma A' + X$. However, as pointed out in [63], the energy resolution of the Babar detector makes two detector-level $M_X^2$

distributions appear to be quite similar (see Figure 8 in [63]). Therefore, in order to quickly estimate the impact of NLO correction on the DP detection limit, we can perform a rescaling by using the total cross-section

$$\varepsilon_{\text{new}} = \varepsilon_{\text{old}} \sqrt{\frac{\sigma_0(e^+e^- \to \gamma A')}{\sigma(e^+e^- \to \gamma A' + X)}} \,. \tag{33}$$

As is reflected in the common $(m_{A'}, \varepsilon)$ plane, that is, after considering the NLO correction, the exclusion limit will be shifted in the $\varepsilon$ direction.

It should be emphasized that Equation (33) is a simple total-rate rescaling estimate rather than a replacement of the official BaBar cut-and-count or likelihood analysis. The shifted curves should therefore be interpreted as a rough estimation of the effect of dark NLO correction. For illustration, in Figure 6, we present the original BaBar limit together with the shifted exclusion limits with NLO correction considered. For the benchmark points shown in the figure, the total-rate rescaling strengthens the limit by about 0.36%, 2.7%, and 6.4% for $(\alpha', r) = (0.1, 3), (0.3, 1)$, and $(0.5, 1/2)$, respectively.

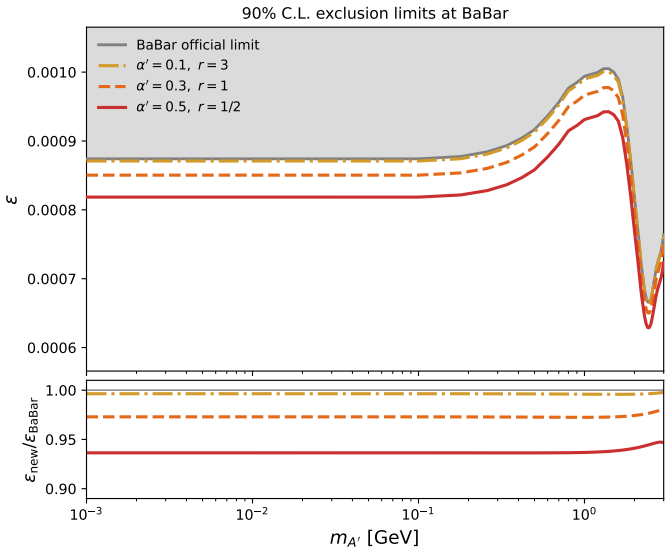



**Figure 6.** Shifted exclusion limits on $(m_{A'}, \varepsilon)$ plane induced by simple cross-section rescaling. Grey is the 90% C.L. exclusion region given in the BaBar report [35], which is based on the tree-level cross-section $\sigma_0$. Colored lines are illustrative of total-rate rescaled limits for $(\alpha', r) = (0.1, 3), (0.3, 1), (0.5, 1/2)$, from top to bottom.

## 5. Conclusions

In this work, we studied the inclusive single dark photon production in an electron–positron collider up to next-to-leading order in the dark sector, within a dark Abelian Higgs model where the dark photon mass is generated by spontaneous symmetry breaking. In addition to the tree-level process $e^+e^- \to \gamma A'$, we included the real emission process $e^+e^- \to \gamma A's$ and the corresponding virtual correction from the dark photon self-energy.

We showed analytically that although both the real and virtual corrections contain infrared divergence in the $m_{A'} \to 0$ limit, their sum is finite at the level of the inclusive cross-section. The resulting dark NLO correction therefore provides an IR-safe prediction for the mono-photon-plus-missing-energy signal.Numerically, we found that this correction can enhance the total cross-section in the low-$m_{A'}$ region and slightly strengthen the current BaBar limit on the kinetic mixing parameter $\varepsilon$.

Our result provides a simple fixed-order description of dark radiation effects in dark photon production, and can serve as a useful supplement to previous studies based on parton shower methods.

**Author Contributions:** Conceptualization, Y.P. and M.Z.; writing, Y.P. and M.Z.; calculating and formal analysis, J.Z. and Y.L.; supervision, Y.P. and M.Z. All authors have read and agreed to the published version of the manuscript.

**Funding:** This work is supported by the Natural Science Foundation of Henan under Grant No. 242300420656, and the National Natural Science Foundation of China (NNSFC) under grant No. 12105118 and 11947118.

**Data Availability Statement:** Data is available upon reasonable request to the authors.

**Conflicts of Interest:** The authors declare no conflicts of interest.

## Notes

[1] Actually, including a non-decoupled dark Higgs when one study DP is a rather natural setting; see [65] for related discussion.

[2] To make this argument more clear, one can consider a light vector-like dark fermion $\chi$, which is charged under $U(1)'$ with charge $Q_\chi$. Then, $A' \to \chi\bar{\chi}$ is the dominant decay channel and $A'$ becomes invisible. We can choose to assign a relatively small $Q_\chi$ (says $1/4$), such that its impact on the total cross-section we intend to calculate is significantly smaller than that of the dark Higgs. Thus, we can simply focus on DP and dark Higgs.

[3] There is another QED IR divergence when $m_e \to 0$ and the photon is collinear with the electron or positron. In this paper, we only focus on the IR divergence when $m_{A'} \to 0$.

[4] In the definition of $\sigma_V$, we also include $\sigma_0$, and thus, here, we subtract 1 to make the correction more visible.

## References

1. Arkani-Hamed, N.; Finkbeiner, D.P.; Slatyer, T.R.; Weiner, N. A Theory of Dark Matter. *Phys. Rev. D* **2009**, *79*, 015014. [CrossRef]
2. Pospelov, M.; Ritz, A. Astrophysical Signatures of Secluded Dark Matter. *Phys. Lett. B* **2009**, *671*, 391–397. [CrossRef]
3. Alves, D.S.M.; Behbahani, S.R.; Schuster, P.; Wacker, J.G. Composite Inelastic Dark Matter. *Phys. Lett. B* **2010**, *692*, 323–326. [CrossRef]
4. Hisano, J.; Matsumoto, S.; Nojiri, M.M. Explosive dark matter annihilation. *Phys. Rev. Lett.* **2004**, *92*, 031303. [CrossRef]
5. March-Russell, J.; West, S.M.; Cumberbatch, D.; Hooper, D. Heavy Dark Matter Through the Higgs Portal. *J. High Energy Phys.* **2008**, *7*, 58. [CrossRef]
6. Arkani-Hamed, N.; Weiner, N. LHC Signals for a SuperUnified Theory of Dark Matter. *J. High Energy Phys.* **2008**, *12*, 104. [CrossRef]
7. Cirelli, M.; Kadastik, M.; Raidal, M.; Strumia, A. Model-independent implications of the $e^{\pm}$, anti-proton cosmic ray spectra on properties of Dark Matter. *Nucl. Phys. B* **2009**, *813*, 1–21. Addendum in *Nucl. Phys. B* **2013**, *873*, 530–533. https://doi.org/10.1016/j.nuclphysb.2013.05.002. [CrossRef]
8. Pospelov, M.; Ritz, A.; Voloshin, M.B. Secluded WIMP Dark Matter. *Phys. Lett. B* **2008**, *662*, 53–61. [CrossRef]
9. Cholis, I.; Dobler, G.; Finkbeiner, D.P.; Goodenough, L.; Weiner, N. The Case for a 700+ GeV WIMP: Cosmic Ray Spectra from ATIC and PAMELA. *Phys. Rev. D* **2009**, *80*, 123518. [CrossRef]
10. Cholis, I.; Finkbeiner, D.P.; Goodenough, L.; Weiner, N. The PAMELA Positron Excess from Annihilations into a Light Boson. *J. Cosmol. Astropart. Phys.* **2009**, *12*, 7. [CrossRef]
11. Rizzo, T.G. Toward UV models of kinetic mixing and portal matter. VI. A more complex dark matter sector? *Phys. Rev. D* **2024**, *110*, 075037. [CrossRef]
12. Abercrombie, D.; Akchurin, N.; Akilli, E.; Maestre, J.A.; Allen, B.; Gonzalez, B.A.; Andrea, J.; Arbey, A.; Azuelos, G.; Azzi, P.; et al. Dark Matter benchmark models for early LHC Run-2 Searches: Report of the ATLAS/CMS Dark Matter Forum. *Phys. Dark Univ.* **2020**, *27*, 100371. [CrossRef]
13. Tan, A. et al. [PandaX-II Collaboration] Dark Matter Results from First 98.7 Days of Data from the PandaX-II Experiment. *Phys. Rev. Lett.* **2016**, *117*, 121303. [CrossRef]
14. Akerib, D.S. et al. [LUX Collaboration] Results from a search for dark matter in the complete LUX exposure. *Phys. Rev. Lett.* **2017**, *118*, 021303. [CrossRef]

15. Aaboud, M.; Aad, G.; Abbott, B.; Abdallah, J.; Abeloos, B.; Abidi, S.H.; AbouZeid, O.S.; Abraham, N.L.; Abramowicz, H.; Abreu, H.; et al. Search for dark matter at $\sqrt{s} = 13$ TeV in final states containing an energetic photon and large missing transverse momentum with the ATLAS detector. *Eur. Phys. J. C* **2017**, *77*, 393. [CrossRef] [PubMed]
16. Aad, G. et al. [ATLAS Collaboration] Search for dark matter in events with a hadronically decaying W or Z boson and missing transverse momentum in $pp$ collisions at $\sqrt{s} = 8$ TeV with the ATLAS detector. *Phys. Rev. Lett.* **2014**, *112*, 041802. [CrossRef] [PubMed]
17. Khachatryan, V.; Sirunyan, A.M.; Tumasyan, A.; Adam, W.; Asilar, E.; Bergauer, T.; Brandstetter, J.; Brondolin, E.; Dragicevic, M.; Erö, J.; et al. Search for dark matter particles in proton-proton collisions at $\sqrt{s} = 8$ TeV using the razor variables. *J. High Energy Phys.* **2016**, *12*, 88. [CrossRef]
18. Aaboud, M. et al. [ATLAS Collaboration] Search for Dark Matter Produced in Association with a Higgs Boson Decaying to $b\bar{b}$ using 36 fb$^{-1}$ of $pp$ collisions at $\sqrt{s} = 13$ TeV with the ATLAS Detector. *Phys. Rev. Lett.* **2017**, *119*, 181804. [CrossRef]
19. Ahdida, C.; Akmete, A.; Albanese, R.; Alt, J.; Alexrov, A.; Anokhina, A.; Aoki, S.; Arduini, G.; Atkin, E.; Azorskiy, N.; et al. The SHiP experiment at the proposed CERN SPS Beam Dump Facility. *Eur. Phys. J. C* **2022**, *82*, 486. [CrossRef]
20. Aubert, B.; Bazan, A.; Boucham, A.; Boutigny, D.; De Bonis, I.; Favier, J.; Gaillard, J.M.; Jeremie, A.; Karyotakis, Y.; Le Flour, T.; et al. The BaBar detector. *Nucl. Instrum. Methods Phys. Res. Sect. A* **2002**, *479*, 1–116. [CrossRef]
21. Abashian, A.; Gotow, K.; Morgan, N.; Piilonen, L.; Schrenk, S.; Abe, K.; Adachi, I.; Alexer J.P.; Aoki, K.; Behari, S.; et al. The Belle Detector. *Nucl. Instrum. Methods Phys. Res. Sect. A* **2002**, *479*, 117–232. [CrossRef]
22. Ablikim, M.; An, Z.H.; Bai, J.Z.; Berger, N.; Bian, J.M.; Cai, X.; Cao, G.F.; Cao, X.X.; Chang, J.F.; Chen, C.; et al. Design and Construction of the BESIII Detector. *Nucl. Instrum. Methods Phys. Res. Sect. A* **2010**, *614*, 345–399. [CrossRef]
23. Adinolfi, M.; Ambrosino, F.; Andryakov, A.; Antonelli, A.; Antonelli, M.; Bacci, C.; Baldini-Ferroli, R.; Bankamp, A.; Bellini, F.; Bencivenni, G.; et al. The tracking detector of the KLOE experiment. *Nucl. Instrum. Methods Phys. Res. Sect. A* **2002**, *488*, 51–73. [CrossRef]
24. Andreas, S.; Donskov, S.V.; Crivelli, P.; Gardikiotis, A.; Gninenko, S.N.; Golubev, N.A.; Guber, F.F.; Ivashkin, A.P.; Kirsanov, M.M.; Krasnikov, N.V.; et al. Proposal for an Experiment to Search for Light Dark Matter at the SPS. *arXiv* **2013**, arXiv:1312.3309. [CrossRef]
25. Banerjee, D. et al. [NA64 Collaboration] Search for invisible decays of sub-GeV dark photons in missing-energy events at the CERN SPS. *Phys. Rev. Lett.* **2017**, *118*, 011802. [CrossRef]
26. Gninenko, S.N. Search for MeV dark photons in a light-shining-through-walls experiment at CERN. *Phys. Rev. D* **2014**, *89*, 075008. [CrossRef]
27. Banerjee, D. et al. [The NA64 Collaboration] Search for vector mediator of Dark Matter production in invisible decay mode. *Phys. Rev. D* **2018**, *97*, 072002. [CrossRef]
28. Chen, J.; Chen, J.Y.; Chen, J.F.; Chen, X.; Fu, C.B.; Guo, J.; He, L.; He, Z.T.; Khaw, K.S.; Li, J.L.; et al. Prospective study of light dark matter search with a newly proposed DarkSHINE experiment. *Sci. China Phys. Mech. Astron.* **2023**, *66*, 211062. [CrossRef]
29. Yan, B. Probing the dark photon via polarized DIS scattering at the HERA and EIC. *Phys. Lett. B* **2022**, *833*, 137384. [CrossRef]
30. Feng, J.L.; Galon, I.; Kling, F.; Trojanowski, S. ForwArd Search ExpeRiment at the LHC. *Phys. Rev. D* **2018**, *97*, 035001. [CrossRef]
31. Abreu, H.; Mansour, E.A.; Antel, C.; Ariga, A.; Ariga, T.; Bernlochner, F.; Boeckh, T.; Boyd, J.; Brenner, L.; Cadoux, F.; et al. The FASER detector. *J. Instrum.* **2024**, *19*, P05066. [CrossRef]
32. The LHCb Collaboration; Alves, A.A., Jr.; Filho, L.M.A.; Barbosa, A.F.; Bediaga, I.; Cernicchiaro, G.; Guerrer, G.; Lima, H.P., Jr.; Machado, A.A.; Magnin, J.; et al. The LHCb Detector at the LHC. *J. Instrum.* **2008**, *3*, S08005. [CrossRef]
33. Banerjee, D. et al. [NA64 Collaboration] Dark matter search in missing energy events with NA64. *Phys. Rev. Lett.* **2019**, *123*, 121801. [CrossRef]
34. Zhang, Y.; Zhang, W.T.; Song, M.; Pan, X.A.; Niu, Z.M.; Li, G. Probing invisible decay of dark photon at BESIII and future STCF via monophoton searches. *Phys. Rev. D* **2019**, *100*, 115016. [CrossRef]
35. Lees, J.P. et al. [BaBar Collaboration] Search for Invisible Decays of a Dark Photon Produced in $e^+e^-$ Collisions at BaBar. *Phys. Rev. Lett.* **2017**, *119*, 131804. [CrossRef]
36. Ablikim, M. et al. [BESIII Collaboration] Dark Photon Search in the Mass Range Between 1.5 and 3.4 GeV/$c^2$. *Phys. Lett. B* **2017**, *774*, 252–257. [CrossRef]
37. Ilten, P.; Thaler, J.; Williams, M.; Xue, W. Dark photons from charm mesons at LHCb. *Phys. Rev. D* **2015**, *92*, 115017. [CrossRef]
38. KLOE-2 Collaboration; Babusci, D.; Badoni, D.; Balwierz-Pytko, I.; Bencivenni, G.; Bini, C.; Bloise, C.; Bossi, F.; Branchini, P.; Budano, A.; et al. Limit on the production of a light vector gauge boson in phi meson decays with the KLOE detector. *Phys. Lett. B* **2013**, *720*, 111–115. [CrossRef]
39. Anastasi, A. et al. [The KLOE-2 Collaboration] Limit on the production of a new vector boson in $e^+e^- \to U\gamma$, $U \to \pi^+\pi^-$ with the KLOE experiment. *Phys. Lett. B* **2016**, *757*, 356–361. [CrossRef]
40. Ilten, P.; Soreq, Y.; Thaler, J.; Williams, M.; Xue, W. Proposed Inclusive Dark Photon Search at LHCb. *Phys. Rev. Lett.* **2016**, *116*, 251803. [CrossRef]

41. Merkel, H. et al. [A1 Collaboration] Search at the Mainz Microtron for Light Massive Gauge Bosons Relevant for the Muon g-2 Anomaly. *Phys. Rev. Lett.* **2014**, *112*, 221802. [CrossRef]
42. Lees, J.P. et al. [BaBar Collaboration] Search for a Dark Photon in $e^+e^-$ Collisions at BaBar. *Phys. Rev. Lett.* **2014**, *113*, 201801. [CrossRef]
43. KLOE-2 Collaboration; Archilli, F.; Babusci, D.; Badoni, D.; Balwierz, I.; Bencivenni, G.; Bini, C.; Bloise, C.; Bocci, V.; Bossi, F.; et al. Search for a vector gauge boson in $\phi$ meson decays with the KLOE detector. *Phys. Lett. B* **2012**, *706*, 251–255. [CrossRef]
44. Aaij, R. et al. [LHCb Collaboration] Search for $A' \to \mu^+\mu^-$ Decays. *Phys. Rev. Lett.* **2020**, *124*, 041801. [CrossRef]
45. Babusci, D. et al. [KLOE-2 Collaboration] Search for light vector boson production in $e^+e^- \to \mu^+\mu^-\gamma$ interactions with the KLOE experiment. *Phys. Lett. B* **2014**, *736*, 459–464. [CrossRef]
46. Batley, J.R. et al. [NA48/2 Collaboration] Search for the dark photon in $\pi^0$ decays. *Phys. Lett. B* **2015**, *746*, 178–185. [CrossRef]
47. Altmannshofer, W.; Urquijo, P.; Altmannshofer, W.; Beaujean, F.; Bell, G.; Beneke, M.; Bigi, I.I.; Bishara, F.; Blanke, M.; Bobeth, C.; et al. The Belle II Physics Book. *Prog. Theor. Exp. Phys.* **2019**, *2019*, 123C01. Erratum in *Prog. Theor. Exp. Phys.* **2020**, *2020*, 029201. https://doi.org/10.1093/ptep/ptaa008. [CrossRef]
48. Aaij, R. et al. [LHCb Collaboration] Search for Dark Photons Produced in 13 TeV $pp$ Collisions. *Phys. Rev. Lett.* **2018**, *120*, 061801. [CrossRef]
49. Sirunyan, A.M. et al. [CMS Collaboration] Search for a Narrow Resonance Lighter than 200 GeV Decaying to a Pair of Muons in Proton-Proton Collisions at $\sqrt{s} = 13$ TeV. *Phys. Rev. Lett.* **2020**, *124*, 131802. [CrossRef] [PubMed]
50. Aad, G. et al. [ATLAS Collaboration] Search for Dark Photons from Higgs Boson Decays via $ZH$ Production with a Photon Plus Missing Transverse Momentum Signature from $pp$ Collisions at $\sqrt{s} = 13$ TeV with the ATLAS Detector. *J. High Energy Phys.* **2023**, *7*, 133. [CrossRef]
51. Aad, G. et al. [ATLAS Collaboration] Search for Dark Photons in Rare $Z$ Boson Decays with the ATLAS Detector. *Phys. Rev. Lett.* **2023**, *131*, 251801. [CrossRef]
52. Aad, G. et al. [ATLAS Collaboration] Combination of Searches for Higgs Boson Decays into a Photon and a Massless Dark Photon Using $pp$ Collisions at $\sqrt{s} = 13$ TeV with the ATLAS Detector. *J. High Energy Phys.* **2024**, *8*, 153. [CrossRef]
53. Aad, G. et al. [ATLAS Collaboration] Search for Light Neutral Particles Decaying Promptly into Collimated Pairs of Electrons or Muons in $pp$ Collisions at $\sqrt{s} = 13$ TeV with the ATLAS Detector. *Eur. Phys. J. C* **2025**, *85*, 335. [CrossRef]
54. Abreu, H. et al. [FASER Collaboration] Search for Dark Photons with the FASER Detector at the LHC. *Phys. Lett. B* **2024**, *848*, 138378. [CrossRef]
55. Falkowski, A.; Ruderman, J.T.; Volansky, T.; Zupan, J. Hidden Higgs Decaying to Lepton Jets. *J. High Energy Phys.* **2010**, *5*, 77. [CrossRef]
56. Biswas, S.; Gabrielli, E.; Mele, B. Dark Photon Searches via Higgs Boson Production at the LHC and Beyond. *Symmetry* **2022**, *14*, 1522. [CrossRef]
57. Batell, B.; Pospelov, M.; Ritz, A. Probing a Secluded U(1) at B-factories. *Phys. Rev. D* **2009**, *79*, 115008. [CrossRef]
58. Cheung, K.; Kim, Y.; Kwon, Y.; Ouseph, C.J.; Soffer, A.; Wang, Z.S. Probing dark photons from a light scalar at Belle II. *J. High Energy Phys.* **2024**, *5*, 94. [CrossRef]
59. Abudinén, F. et al. [Belle II Collaboration] Search for a Dark Photon and an Invisible Dark Higgs Boson in $\mu$+$\mu$- and Missing Energy Final States with the Belle II Experiment. *Phys. Rev. Lett.* **2023**, *130*, 071804. [CrossRef]
60. Anastasi, A. et al. [KLOE-2 Collaboration] Search for dark Higgsstrahlung in $e^+e^- \to \mu^+\mu^-$ and missing energy events with the KLOE experiment. *Phys. Lett. B* **2015**, *747*, 365–372. [CrossRef]
61. Lees, J.P. et al. [BABAR Collaboration] Search for Low-Mass Dark-Sector Higgs Bosons. *Phys. Rev. Lett.* **2012**, *108*, 211801. [CrossRef]
62. Jaegle, I. Search for the dark photon and the dark Higgs boson at Belle. *Phys. Rev. Lett.* **2015**, *114*, 211801. [CrossRef] [PubMed]
63. Li, S.; Yang, J.M.; Zhang, M.; Zhang, Y.; Zhu, R. Unraveling dark Higgs mechanism via dark photon production at an $e^+e^-$ collider. *J. High Energy Phys.* **2026**, *1*, 71. [CrossRef]
64. Acanfora, F.; Kahlhoefer, F. Dark Higgs-strahlung at Belle II: A distinctive dark sector signature with displaced vertices and missing energy. *J. High Energy Phys.* **2025**, *12*, 87. [CrossRef]
65. Li, S.; Yang, J.M.; Zhang, M.; Zhu, R. Theoretical bounds on dark Higgs mass in a self-interacting dark matter model with U(1)′. *Phys. Rev. D* **2025**, *111*, 035005. [CrossRef]
66. Buschmann, M.; Kopp, J.; Liu, J.; Machado, P.A.N. Lepton Jets from Radiating Dark Matter. *J. High Energy Phys.* **2015**, *7*, 45. [CrossRef]
67. Kim, M.; Lee, H.S.; Park, M.; Zhang, M. Examining the origin of dark matter mass at colliders. *Phys. Rev. D* **2018**, *98*, 055027. [CrossRef]
68. Chen, J.; Ko, P.; Li, H.N.; Li, J.; Yokoya, H. Light dark matter showering under broken dark $U(1)$—Revisted. *J. High Energy Phys.* **2019**, *1*, 141. [CrossRef]
69. Chigusa, S.; Yamazaki, M. Quantum simulations of dark sector showers. *Phys. Lett. B* **2022**, *834*, 137466. [CrossRef]

70. Bierlich, C.; Chakraborty, S.; Desai, N.; Gellersen, L.; Helenius, I.; Ilten, P.; Lönnblad, L.; Mrenna, S.; Prestel, S.; Preuss, C.T.; et al. A comprehensive guide to the physics and usage of PYTHIA 8.3. *SciPost Phys. Codebases* **2022**, *8*. [CrossRef]
71. Dudal, D.; van Egmond, D.M.; Guimarães, M.S.; Holanda, O.; Mintz, B.W.; Palhares, L.F.; Peruzzo, G.; Sorella, S.P. Some remarks on the spectral functions of the Abelian Higgs Model. *Phys. Rev. D* **2019**, *100*, 065009. [CrossRef]
72. Kinoshita, T. Mass singularities of Feynman amplitudes. *J. Math. Phys.* **1962**, *3*, 650–677. [CrossRef]
73. Lee, T.D.; Nauenberg, M. Degenerate Systems and Mass Singularities. *Phys. Rev.* **1964**, *133*, B1549–B1562. [CrossRef]

**Disclaimer/Publisher's Note:** The statements, opinions and data contained in all publications are solely those of the individual author(s) and contributor(s) and not of MDPI and/or the editor(s). MDPI and/or the editor(s) disclaim responsibility for any injury to people or property resulting from any ideas, methods, instructions or products referred to in the content.